CLM-P630

UKAEA

Preprint

MAGNETIC EFFECTS IN HIGH CURRENT ION BEAMS

G. A. COTTRELL

CULHAM LABORATORY
Abingdon Oxfordshire

1981

CLM-P 630

MAGNETIC EFFECTS IN HIGH-CURRENT ION BEAMS

G. A. Cottrell

Culham Laboratory, Abingdon, Oxon, OX14 3DB, UK.
(Euratom/UKAEA Fusion Association)

ABSTRACT

It is known that, in intense ion beams being developed for use in neutral injection, the space-charge of the ions is almost totally compensated by electrons. In the limit of total compensation, it is shown that there is a critical ion current, I_c, above which transport is no longer emittance but magnetic self-field dominated. A Monte-Carlo model of beam neutralisation in the presence of the self-field is presented and applied to the example of the JET injectors. Results show a foreshortening of the injector focus, a rise in beamlet emittance and an increase in the angular divergence (of order 0.1^0) in high current neutral injectors. It is shown that, because of stochastic neutralisation effects, there is a fundamental limit to the ability to focus an injector uniquely.

(Accepted for publication in Review of Scientific Instruments)

May 1981

1. INTRODUCTION

The additional plasma heating requirements (by fast atom injection) of the next generation of Tokamak experiments (e.g. the Joint European Torus project) have led to the development of high current (I $\simeq$ 60 ampere equivalent) neutral beams of H-atoms at energies typically $V_b \simeq 80$ keV per nucleon. Such large beams are produced by parallel acceleration of many smaller 'beamlets' of hydrogen ions which are then partially converted to neutral atoms by transporting them through a charge-exchange gas cell or neutraliser. In order to achieve a high power transmission to the target plasma (via ducts of limited angular acceptance) not only should the beam steering be well defined but the angular divergence of the super-beam must be minimised. This implies that the beam must have a high degree of space-charge compensation such that in the limit it could be emittance dominated. However, in this limit account must also be taken of the self-magnetic forces which, in an uncompensated beam, are $\sim v_b^2/c^2$ lower in magnitude than the space-charge forces (where v_b is the beam velocity). In this paper we consider the role of the self-field in high current beams and present analyses of both the un-neutralised ion beam transport and the neutral beam transport using a numerical Monte-Carlo model.

2. THE BEAM ENVELOPE

An ion beam propagating in a region having no external fields may be viewed as a drifting gas in which the shape of the boundary of the beam, or beam envelope, is controlled by three main processes. Firstly, because the particles are similarly charged, they tend to repel each other; this causes a growth in the beam size with propagation distance. The second controlling factor arises from the beam emittance, a quantity similar to beam entropy and related, fundamentally, to the finite temperature of the extracted ions. The third factor comes from the fact that the beam of particles constitutes a current and hence generates a self-magnetic field; ions moving in this field will be guided towards the beam axis, thus giving rise to a beam-pinch.

In order to ascertain the dominant process in intense ion beams being developed for use in controlled thermonuclear fusion research, we can use the beam envelope equation for a circularly symmetric beam (Kapchinskiy and Vladimirskiy 1959), Lawson (1978)):

$$\frac{d^2a}{dz^2} - \frac{\varepsilon^2}{a^3} - \frac{\langle E\rangle}{2V_b} + \frac{v_b \langle B\rangle}{2V_b} = 0. \qquad (1)$$

where ε is the emittance, $\langle E\rangle$ and $\langle B\rangle$ the rms electric and magnetic fields respectively,

a the envelope radius, and V_b the beam energy. In this form equation (1) is applicable to a single beam where the envelope radius is defined as the rms radius (Holmes 1979a); this situation is relevant to a neutral injection system in which the beamlets are merged. The relative importance of the three terms in equation (1) may be determined from the dimensionless parameters δ_1 (Evans and Warner 1971) and δ_2 where

$$\delta_1 = \frac{a \langle E \rangle}{2T_i} \tag{2}$$

and

$$\delta_2 = \frac{a\, v_b \langle B \rangle}{2T_i} \tag{3}$$

where T_i is the temperature of the extracted ions. Equations (2) and (3) give, respectively, the ratios of the space-charge-to-emittance and self-field-to-emittance terms. For a beam with gaussian profile (having 1/e width equal to a), the rms electric field is given by

$$\langle E \rangle = \frac{0.199\, \phi_w}{a} \tag{4}$$

(Holmes 1979b), and the rms magnetic field by

$$\langle B \rangle = \frac{0.63\, \mu_0 I}{2\pi a} \tag{5}$$

where ϕ_w is the plasma potential of the beam with respect to the edge and I is the beam current.

Experiments on single beamlets have shown that plasma potentials as low as $\phi_w \sim 20$ V may be attained and, under similar experimental conditions (Cottrell and Holmes 1980), measurements of beamlet emittance has implied ion temperatures, $T_i \simeq 0.3$ eV. These values give $\delta_1 \sim 6$, showing that a high degree of space-charge compensation is achieved and that the beam is almost emittance dominated. The scaling of plasma potential with beam radius (Green 1977, Osher 1977, Holmes 1979a) indicates that, for multiple beamlets, the emittance term will dominate over the space-charge term.

However, in this limit the self-field term may be more important than the emittance term since, for protons, we may define a critical current

$$I_c = 36 \left(\frac{V_b}{\text{keV}}\right)^{-\frac{1}{2}} \left(\frac{T_i}{\text{eV}}\right) \text{Amps} \tag{6}$$

at which the parameter δ_2 is equal to unity where

$$\delta_2 = 0.03 \left(\frac{I}{A}\right) \left(\frac{eV}{T_i}\right) \left(\frac{V_b}{keV}\right)^{\frac{1}{2}} \tag{7}$$

Figure 1 shows the variations of I_c with V_b. For currents $I > I_c$ beam transport is self-field dominated and for $I < I_c$ it is emittance limited. As an example, the requirements for the JET beamline are I = 60 A (of ions) at V_b = 80 keV; this point lies in the self-field dominated regime in Figure 1 and, using (7), we derive $\delta_2 = 54$.

2.1 Self-Pinch of the Ion Beam

We next examine the properties of ion beam transport in the self-field ($\delta_2 >> \delta_1$) regime. In the case of an ion beam having an infinite (mechanically defined) focal length, formed by many parallel beamlets, integration of equation (1) in the paraxial approximation gives the solution for the beam envelope

$$a(z) = a_0 - \frac{e\mu_0 I z^2}{4\pi a_0 m v_b} \tag{8}$$

where a_0 is the initial beam radius. Differentiation of equation (8) with respect to z gives the inward pinch-angle

$$a' = \frac{da}{dz} = \frac{-e\mu_0 j_+ a_0 z}{2mv_b} \tag{9}$$

where the current density is j_+. Equation (9) shows that the system has the property of a converging lens with a focal length which depends on the ion beam propagation distance, z.

In a neutral beam injector the ion beam is partially converted to neutral atoms by allowing it to propagate in a gas-cell (neutraliser) in which charge-exchange reactions take place. The fraction, f_+, of the beam remaining as ions after traversing a gas target thickness

$$\pi = \int_0^z n_g(z)\, dz \tag{10}$$

is a monotonically decreasing function of z

$$f_+ = \frac{1}{(\sigma_c + \sigma_s)} \left[\sigma_s + \sigma_c \exp\left(-\pi(\sigma_c + \sigma_s)\right)\right] \tag{11}$$

where σ_c and σ_s are, respectively, the atomic cross-sections for conversion of an ion to a neutral and the converse process (Allison 1958), and $n_g(z)$ is the

gas density in the neutraliser. Because the ion beam current depends on propagation distance through the neutraliser, it is important to solve equation (9) with

$$j_+ (z) = j_+ (o)\, f_+ \qquad (12)$$

in order to calculate the ion beam envelope in a neutral injector.

Accordingly, equations (8) - (12) were solved numerically assuming JET beam parameters (Table I), molecular gas flow in the neutraliser, a mechanically defined injector focal length of 8 metres and a circular-equivalent source radius a_0 equal to 16 cm. Results are shown in Figure 2 for the cases of (i) I = 0, (ii) with a gas target thickness of 300 millitorr cm, and (iii) no neutraliser gas being present. It can be seen that, in the 'neutralised' case (ii), the envelope radius is significantly distorted by the self-field and, at the position of the deflexion magnet ($z \simeq 4$ m), the beam envelope has pinched significantly. At z = 4 m the radius of the unneutralised beam is reduced from its nominal value of a = 8 cm (curve i) to a = 6.5 cm (curve ii). This implies that the ion beam power density should rise by $\simeq$ 51%.

3. MONTE-CARLO ANALYSIS OF THE NEUTRALS

A beam ion injected into the gas-cell may make several charge-changing collisions along its path during which, as an ion, it is accelerated radially towards the beam axis or, whilst a neutral, it moves in a straight path at constant velocity. Because the mean free path for the neutralisation is typically of the order of the length of the gas-cell, there is considerable indeterminacy about the location of the neutralising collisions, and therefore, for a complete analysis, stochasic effects must be taken into account. It is, however, instructive to consider the fate of any ions which become neutralised just as they emerge from the neutraliser. In the example shown in Figure 2 the slope, a', of curve (ii) is -0.024 at z = 2 m, implying that if an ion were neutralised there its focal point would be 6.7 m, i.e. smaller than the mechanically defined focus by 1.3 m. Since most of the neutrals will be created earlier in the neutraliser, this example represents the worst case.

3.1 The Model

In order to quantify the stochastic processes, a numerical Monte-Carlo analysis has been applied to the problem of neutralisation in the gas-cell. In the model, the trajectories of single particles were followed from the source to

the exit point of the neutraliser. The length, L_N, of the neutraliser was divided into 100 cells (each of length Δz) inside which the gas density was taken to be constant. In each cell a decision was taken to determine if the particle was an ion or a neutral. The decision depended on whether $n_g(z)\ \sigma_c\ \Delta z < R$ (for ions) or $n_g(z)\ \sigma_s\ \Delta z < R$ (for neutrals) where R was a computer-generated pseudo-random number distributed uniformly between 0 and 1. Depending on the outcome of the trial, the relevant equation of motion was solved over Δz. In the case of ions, the new co-ordinates in the (n+1)th cell are given by

$$\left.\begin{aligned} a_{n+1} &= a_n - \frac{\mu_0 e\, I(z)\, \Delta z^2}{4\pi\, r(z)\, m_i\, v_b} + a_n' \Delta z \\ a'_{n+1} &= a'_n - \frac{\mu_0 e\, I(z)\, \Delta z}{2\pi\, r(z)\, m_i\, v_b} \end{aligned}\right\} \qquad (13)$$

where

$$I(z) = \pi a_0^2\, j_+(o)\, f_+, \text{ and} \qquad (14)$$

$$r(z) = a_0 (1 - z/f_L) \qquad (15)$$

where a_0 and f_L are, respectively, the initial particle radius and the (mechanically defined) focal length.

For a close-coupled neutraliser with gas injection operating in the molecular gas-flow regime, the density profile is given by

$$\left.\begin{aligned} n_g &= n_g^0 \quad , \quad 0 \le z \le L_F \\ n_g &= n_g^0 \left[\frac{L_N - z}{L_N - L_F}\right], \ L_F \le z \le L_N \end{aligned}\right\} \qquad (16)$$

and zero elsewhere; L_F is the gas feed point. The gas density profile is shown in Figure 3 together with the experimental layout and co-ordinate convention.

Equations (13) - (16) were solved numerically using the Culham Prime-500 computer for (typically) up to 1000 test particles per trial run. Only neutrals exiting the neutraliser were subsequently followed.

3.2 Example Calculations

The analysis was applied to two neutral injector systems, the DITE (phase II)

injectors and the injectors proposed for the Joint European Torus (JET) experiment. Adopted parameters for these systems are shown in Table I.

3.2.1 The JET injectors

The distribution of actual focal lengths calculated for the neutrals is shown in Figure 4 for several different values of the peak gas density, n_g^0. As n_g^0 was raised from below the value for 85% equilibrium target thickness (equivalent to $n_g^0 = 6.4 \times 10^{19}\ m^{-3}$) to above this value two changes occurred: firstly, the neutral yield rises (as expected from equation (11)), and secondly the scatter in the distribution decreases. The half-width at $^1/_e$ of the maximum of each distribution is plotted in Figure 5 as a function of n_g^0. Figure 4, however, shows that the particles fall short of the mechanically defined focal length by up to 1.2 m. At the normal operating point of the injector ($n_g^0 = 6.4 \times 10^{19}\ m^{-3}$), the mean focal length is $\bar{f}_L = 7.5$ m with an rms deviation of 30 cm.

The spread in the steering angle distribution of the neutrals formed from ions launched from the edge of the circular-equivalent ($a_0 = 16$ cm) source constitutes an extra angular divergence of 0.07^0 at this operating point.

3.2.2 The DITE (phase II) injectors

The analysis has also been applied to the DITE injector system for comparison with the JET system. The distribution of focal lengths is shown in Figure 6, plotted for several values of n_g^0. In this example neutralisation is obtained by the use of source gas alone, a situation simulated by setting $L_F = 0$ in the model. Results show that the neutrals fall short of the intended focal length by up to 30 cm. Magnetic effects are less important here than in the JET case. The additional angular divergence of the neutrals formed from ions launched from the edge of the circular-equivalent ($a_0 = 9.6$ cm) source is 0.04^0 at $n_g^0 = 3 \times 10^{19}\ m^{-3}$.

3.3 Stochastic Effects and Emittance Growth

If ions are injected into the gas-cell with *identical* initial (a_0, a_0') co-ordinates they will emerge, as neutrals, from the cell each with *different* final (a, a') co-ordinates, depending on exactly where the charge-changing collisions occurred for each particle. This special effect occurs only in the presence of electric or magnetic fields in the neutraliser. Thus, in the presence of the self-field of the beam, this effect constitutes a form of scattering producing a cone of particles exiting the neutraliser and therefore introduces an extra component of beam emittance. The physical basis of this non-Liouvillian disordering process is precisely the lack of information about the location of the charge-changing

processes. If, for example, all the neutrals were formed at the same position there would be no growth in emittance, even when fields are present.

A plot of the emittance diagram (in phase-space) is shown in Figure 7 for the JET case; in this example there was no mechanical steering ($f_L = \infty$) and $n_g^0 = 6.4 \times 10^{19}\ m^{-3}$. The axis of the diagram is tilted with a negative slope in the (r,r′) plane, indicating the self-focussing effect. The characteristic 'bow-tie' shape arises from the fact that the spread in r′ (defined by the $^1/_e$ points of the distribution) increases linearly with r. The normalised emittance is defined as

$$\varepsilon_n = \frac{\beta A}{\pi} \qquad (17)$$

where A is the area in phase-space (enclosed by the $^1/_e$ contour) and is shown in Figure 7 by the shaded region. The variation of ε_n with n_g^0 is shown in Figure 8. The normalised emittance decreases with n_g^0 because the beam particles suffer increasingly similar deflections as the average number of charge-changing collisions per particle rises.

In this example of a circularly-symmetric beam, ~ 250 beamlets contribute to the total normalised emittance; the normalised emittance per beamlet is 2.2×10^{-3} π mm mrad, approximately 10% of the value measured in a H_e^+ ion beamlet (Holmes and Inman 1979). In the case of a mixed-species hydrogenic beamlet the observed normalised emittance is ~ 5 times larger than for a helium beam; part of this excess comes from the collisional break-up of the H_2^+ and H_3^+ ions which give the beam a higher transverse ion temperature. In the case of the mechanically focussed JET beam, the ensuing amplification of the self-field in the neutraliser increases the transverse velocity spread of the neutrals by approximately 20% over the case shown in Figure 7.

In practical neutral injectors, the dominant emittance comes from the ion temperature in the plasma generator. However the stochastic effect in the presence of the beam self-field does impart an irreducible 'base' emittance to a neutralised beam.

3.4 Rectangular Beams

In the two examples discussed above, the rectangular extraction areas were approximated by equivalent area circular sources. We now consider additional effects related to the source geometry.

For simplicity, consider the behaviour of beamlets located on the two planes of symmetry in Figure 9. The Lorentz force, F_y, acting on a charged particle emerging from the point (0,0) (due to the whole array of beamlets) is

$$F_y = e\, v_b\, B_x \tag{18}$$

where, by symmetry, we need only calculate the y-component of the force. The incremental x-component of the field due to current element $j_+\, dx\, dy$ at point (x,y) on Figure 9 is

$$dB_x = \frac{\mu_0\, j_+ \cos\alpha\, dx\, dy}{2\pi (x^2 + y^2)^{\frac{1}{2}}} \tag{19}$$

and the total x-component is

$$B_x = \frac{\mu_0\, j_+}{2\pi} \int_0^{2b} \int_{-a}^{a} \frac{y\, dx\, dy}{(x^2 + y^2)} \tag{20}$$

where a and be are, respectively, the minor dimensions of the source and we have assumed the current density to be uniform over the source. Equation (20) can be evaluated using standard formulae (Abramowitz and Stegun 1970) giving

$$B_x = \frac{\mu_0\, j_+ a}{\pi} \left[\frac{\arctan\,(a/2b)}{(a/2b)} - \tfrac{1}{2}\, \ell n \left[\frac{(a/2b)^2}{1 + (a/2b)^2} \right] \right] \tag{21}$$

For a slab-beam where $(a/2b) \to 0$, equation (21) becomes $B_x = \mu_0\, j_+ b$, in agreement with the result of application of Ampere's circuital law.

In the JET source, $(a/2b) = 0.2$ for a beamlet at (0,0) and is equal to 1.25 for a beamlet at (±a,b). These two cases give respectively $B_x = 0.83\, \mu_0\, j_+ a$ and $b_x = 0.31\, \mu_0\, j_+ a$. Application of the Monte-Carlo analysis to these two cases gave the distributions shown in Figure 10 assuming the same (f_L = 8 m) (mechanically defined) focus in both planes. The beamlet on the long-axis is focussed to a mean focal length 7.1 (± 0.4 s.d.) m, significantly shorter than in the circular approximation. The beamlet on the short-axis, however, focusses at 7.6 (± 0.16 s.d.) m, closer to the mechanical focus than in the circular approximation. Beamlets not lying on the planes of symmetry will have foci between these two limits; also they will be weakly aberrated, because they are not focussed directly to the z-axis. The maximum additional angular beamlet divergence in this example is 0.1^0.

4. DISCUSSION

So far we have only considered the effects of the self-magnetic field of the ion beam on transport. However, currents other than the beam current are present which, even if the neutraliser duct is magnetically shielded from external fields, may influence the transport. The ion/neutral beam, as it propagates in the neutraliser, produces both slow ions and electrons by charge exchange and ionisation. It is generally assumed that the currents of these two components are purely radial and hence do not contribute to currents which may produce azimuthal magnetic fields (Green 1977). The return paths for these currents are in the metal walls of the neutraliser; if, for example, the return paths were non-coaxial then the associated fields could result in extra aberrations in the self-field 'lens', which would influence the ion optics. The effects of beam deflection in neutralisers due to stray external magnetic fields has been considered by Conrad (1978). However, unlike these effects, the effects of the self-field considered here cannot be eliminated by magnetically shielding the neutraliser. Another possibility is that in the beam-plasma the electron current flow pattern may be modified by deliberately changing the potential of various elements of the neutraliser. This would give, in principle, the possibility of producing axial electron currents which would modify the azimuthal magnetic field and hence the focussing of the total ion beam. Such currents may even be augmented by electron injection from heated filaments. The under-focussing effect in neutral injectors due to the self-focussing field could, in principle, be compensated for by changing the grid curvature (in the sense of mechanically over-steering the beam). In the case of a circularly-symmetric source, the correction is considerably simpler to apply than in the case of a rectangular source. This is because, in the latter case, the steering correction is not a simple function of radius but is a complex function of position on the rectangular grid.

It is useful to consider the scaling of the self-magnetic pinch effect with beam energy. We can do this for a neutral injector operated at (a) constant perveance, and (b) constant current. Neglecting neutralisation effects, the inward pinch angle (at constant z), given by equation (9) scales as

a) $a' \propto -V_b$ (at constant perveance),

and b) $a' \propto -V_b^{-\frac{1}{2}}$ (at constant current).

In the first case the variation will be even more pronounced when neutralisation

effects are included. This is because both the ion fraction, f_+, and the length, L_N, of the neutraliser increase with V_b.

In summary, it is likely that, due to the high degree of space-charge compensation and low ion temperatures known to be present in high current beams, beam transport will not be emittance limited but instead will be dominated by self-magnetic field effects. These effects reduce the focal length of an injector significantly, and cause the unneutralised ion beam to be pinched more strongly than the neutral beam. In high current neutral beam experiments where (a) the residual ion beam is not deflected away, and (b) propagation distances in the order of several metres are involved, this differential effect between the ion and neutral beams may have to be taken into account.

I thank Drs. T. S. Green and A. J. T. Holmes for discussions.

TABLE I

Parameters for two Neutral Beam Sources

	DITE (II)	JET
Ion current, I (A)	30	60
Extraction voltage, V_b (keV)	25	80
Extraction area, a x b (cm^2)	8 x 36	18 x 45
Average current density, j_+ (mA cm^{-2})	104	74
Geometrical focal length, f_L (m)	3.6	8.0
Neutraliser length, L_N (m)	1.0	2.0
Gas feed point, L_F (m)	0	1.0
Peak gas density, n_g^0 (m^{-3})	3×10^{19}	6.4×10^{19}

REFERENCES

Abramowitz, M., and Stegun, I. A. Handb. of Math. Funct., Dover Publ. Inc., N.Y., 83, (1970).

Allison, S. K., Rev. Mod. Phys., 30, 1137, (1958).

Conrad, J. R., J. Appl. Phys., 49(7), 3656, (1978).

Cottrell, G. A., and Holmes, A. J. T., Inst. Phys. Conf. Ser. No. 54, 13-19, (1980).

Evans, L., and Warner, D., IEEE Trans. Nuc. Sci., NS-18, 1068-1070, (1971).

Green, T. S., Proc. Symp. on Prod. and Neut. of Negative Ion Beams, Brookhaven Nat. Lab., N.Y., 228-230, (1977).

Holmes, A. J. T. Phys. Rev. A, 19, 389-407, (1979a).

Holmes, A. J. T. Radiation Effects, 44, 47-58, (1979b).

Holmes, A. J. T., and Inman, M., Conf. 'Linear Accel.', Brookhaven, (1979).

Kapchinskiy, I. M., and Vladimirskiy, V. V., Proc. Int. Conf. on High Energy Accelerators. (Geneva: CERN), 274, (1959).

Lawson, J., The Physics of Charged Particle Beams. O.U.P. Oxford, U.K. (1978).

Osher, J. E., Inst. Phys. Conf. Ser. No. 38, 201-211, (1977).

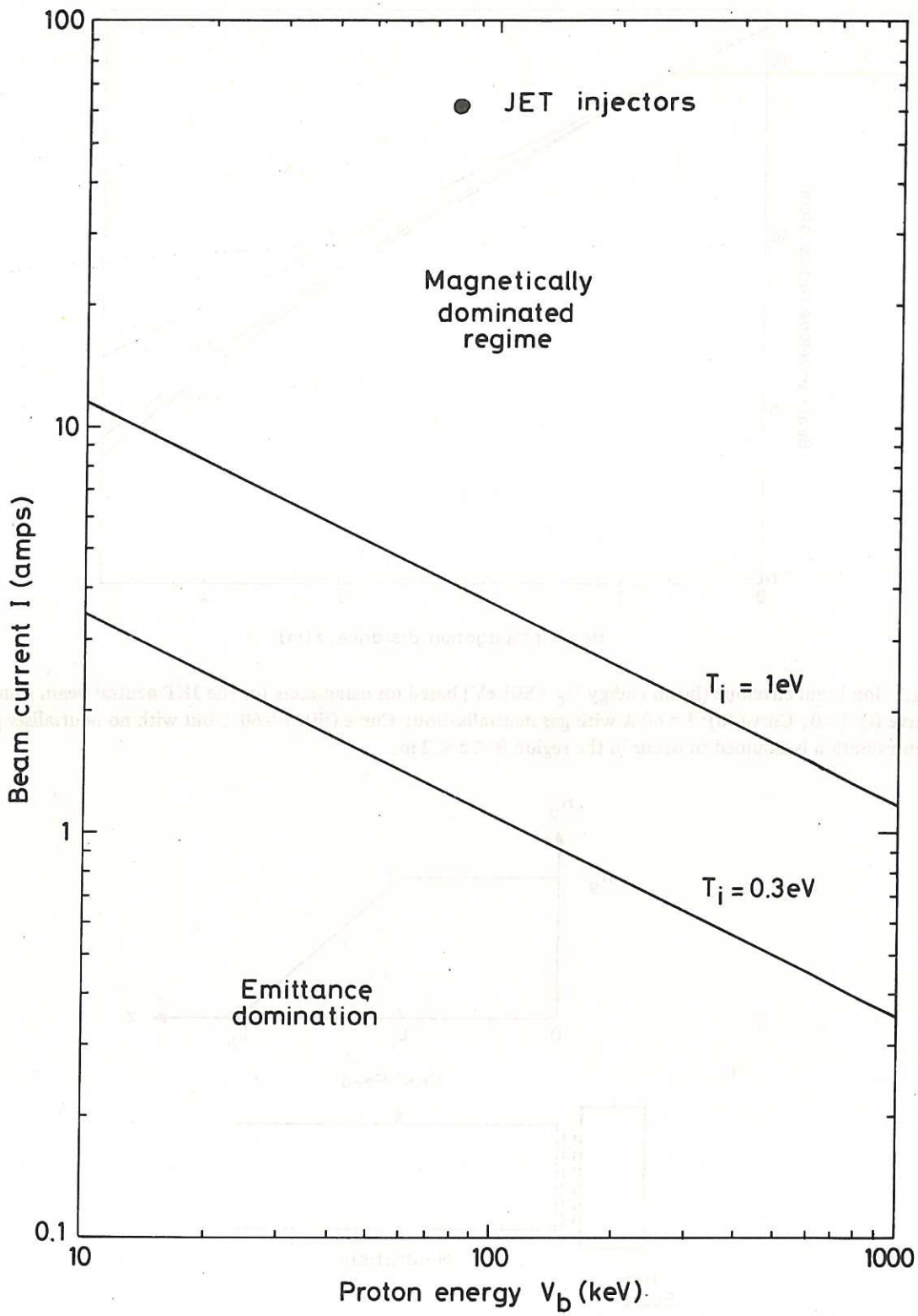

Fig.1 Plot of ion beam current I against beam energy V_b for a neutral injector showing critical current lines for two extracted ion temperatures. Points above the lines lie in the magnetically dominated transport region; those below lie in the emittance dominated transport region.

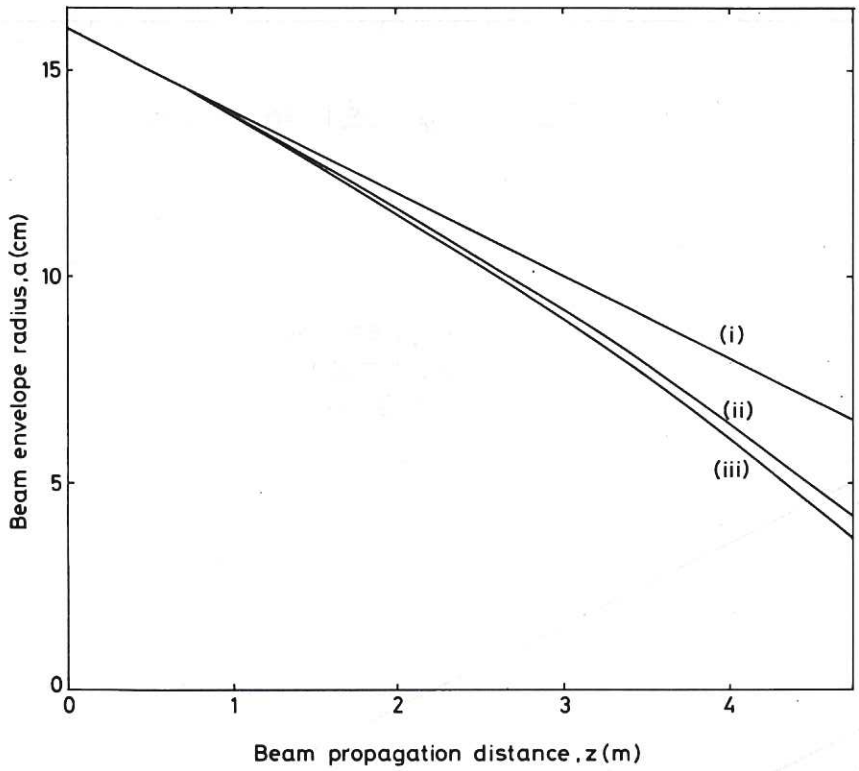

Fig.2 Ion beam envelope (beam energy $V_b = 80$ keV) based on parameters for the JET neutral beam source. Curve (i): I = 0; Curve (ii): I = 60 A with gas neutralisation; Curve (iii): I = 60 A but with no neutraliser gas. Neutralisation is assumed to occur in the region $0 < z < 2$ m.

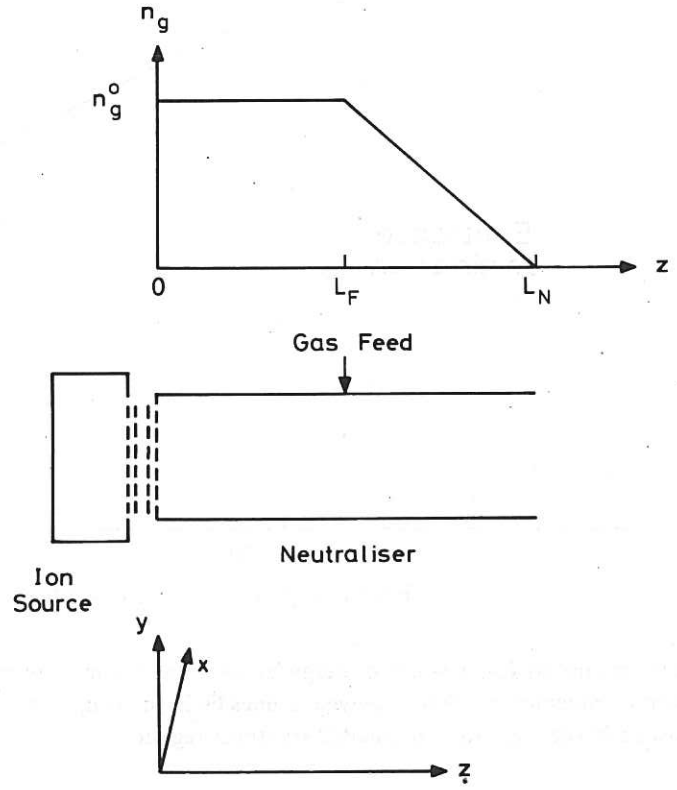

Fig.3 Upper: gas density profile in the neutraliser; Centre: schematic layout of experimental neutral beam source showing position at which gas is injected in the neutraliser; Lower: coordinate system.

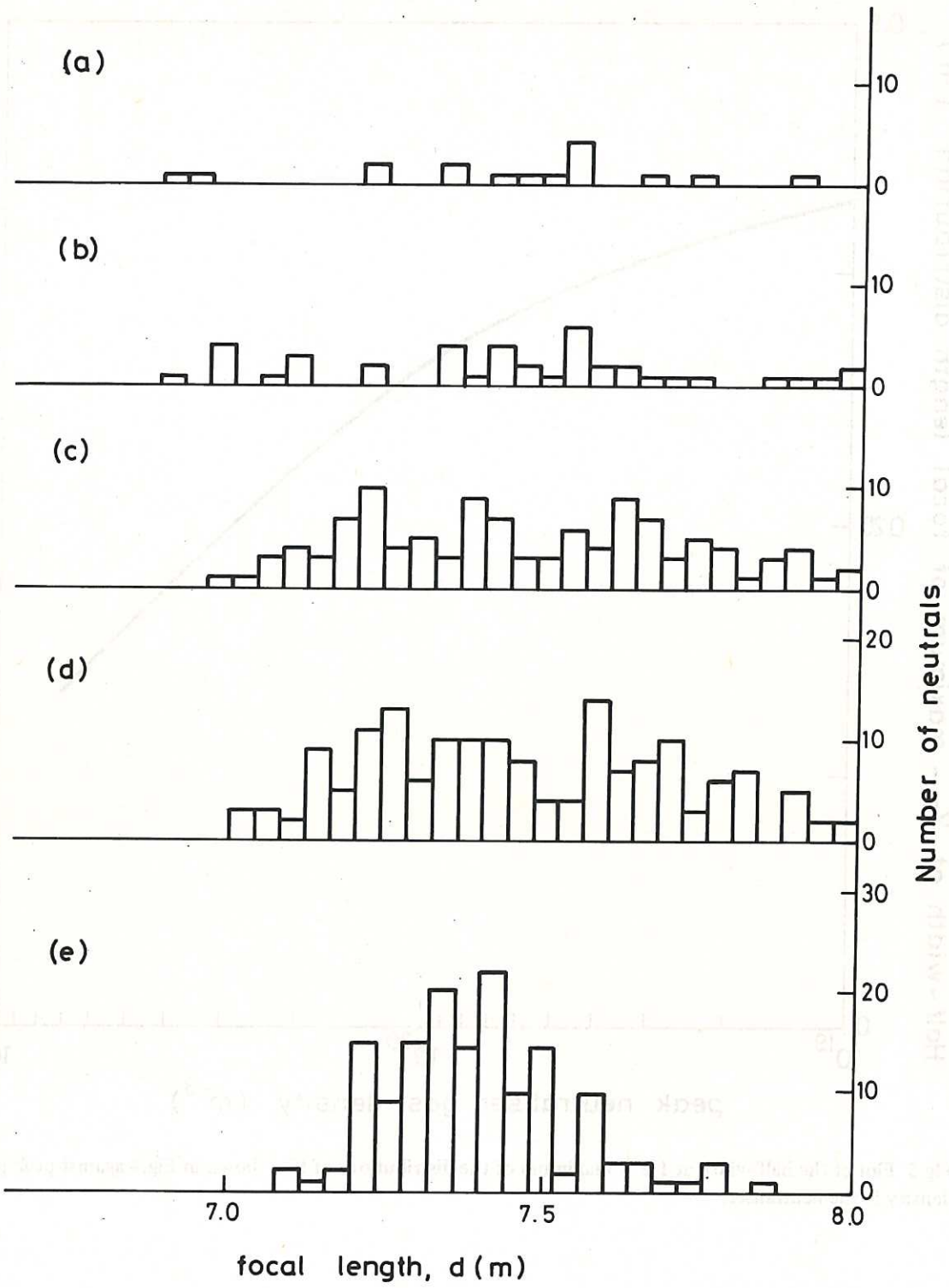

Fig.4 Results of Monte-Carlo calculation for the JET neutral injectors showing the distribution of neutral particle foci for several different peak gas densities in the neutraliser. The peak densities of H_2 are: (a) 5×10^{18} m^{-3}; (b) 10^{19} m^{-3}; (c) 5×10^{19} m^{-3}; (d) 10^{20} m^{-3}; and (e) 5×10^{20} m^{-3}. The mechanically defined focus was $f_L = 8{\cdot}0$ m.

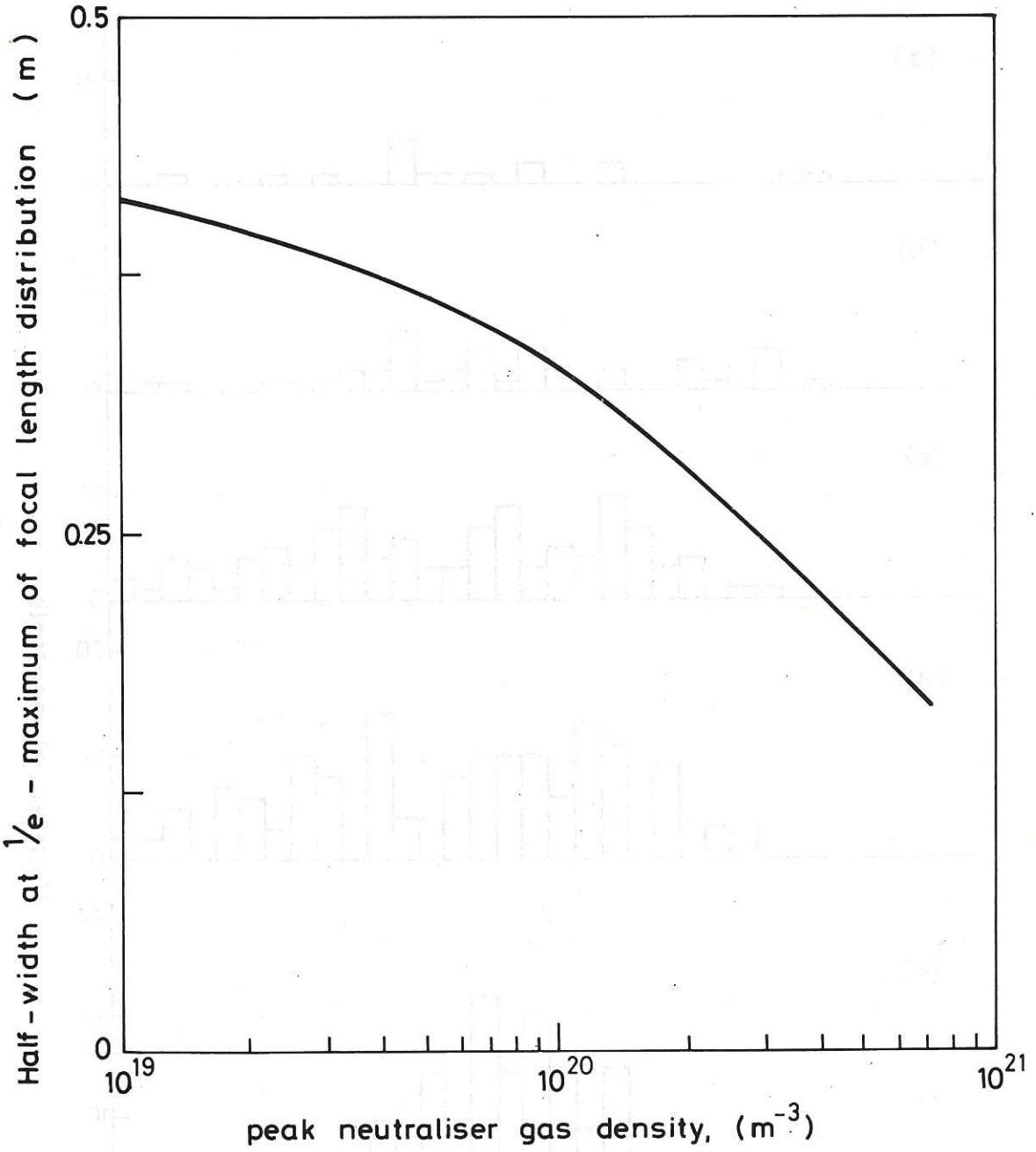

Fig.5 Plot of the half-width at 1/e – maximum of the distributions of foci shown in Fig.4 against peak gas density in the neutraliser.

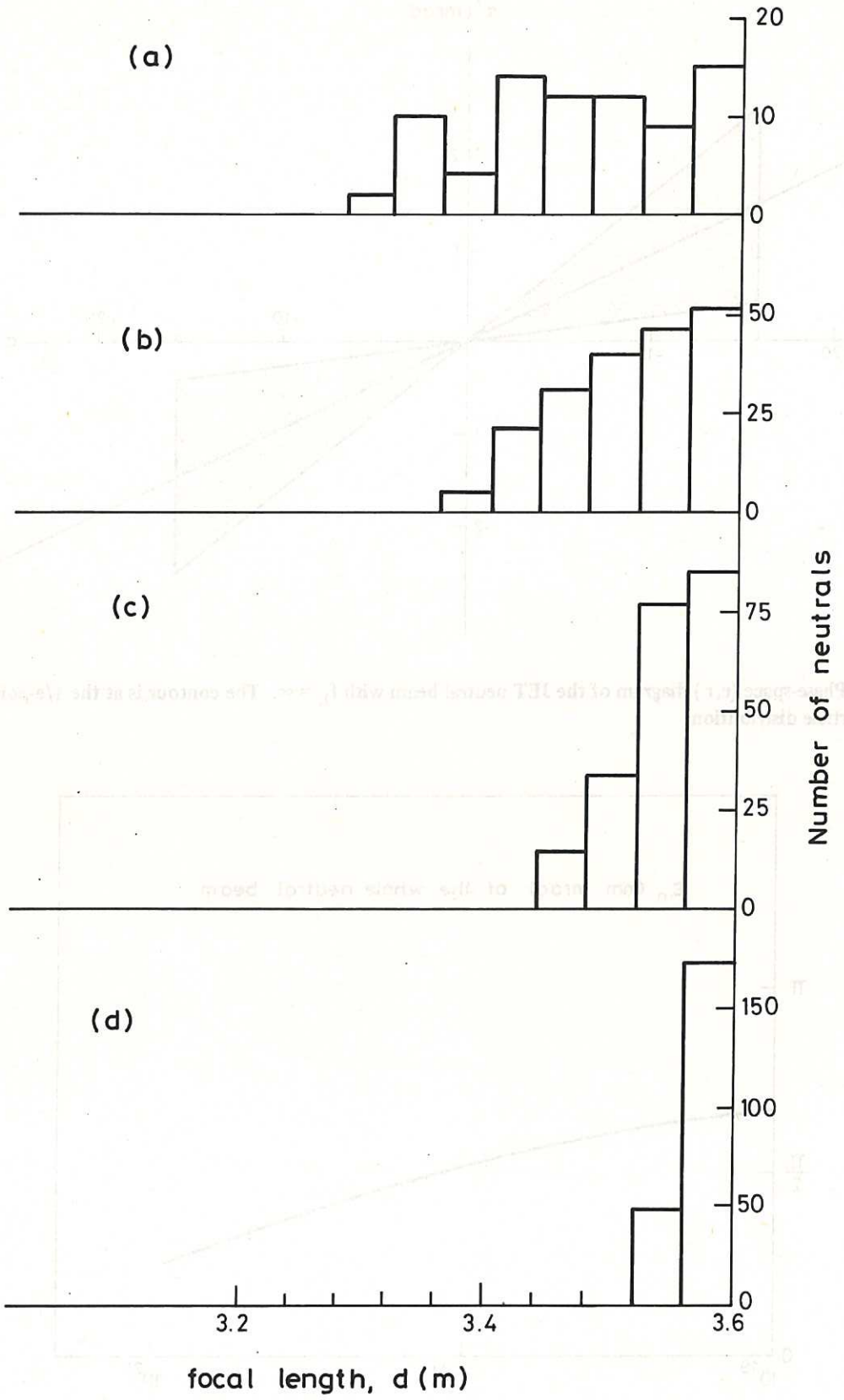

Fig.6 Results of Monte-Carlo calculation for the DITE (Phase II) injectors showing the distribution of neutral particle foci for several different peak gas densities in the neutraliser. The peak H_2 densities are: (a) 10^{19} m^{-3}; (b) 5×10^{19} m^{-3}; (c) 10^{20} m^{-3}; and (d) $3{\cdot}2 \times 10^{20}$ m^{-3}. The mechanically defined focus was at $f_L = 3{\cdot}6$ m.

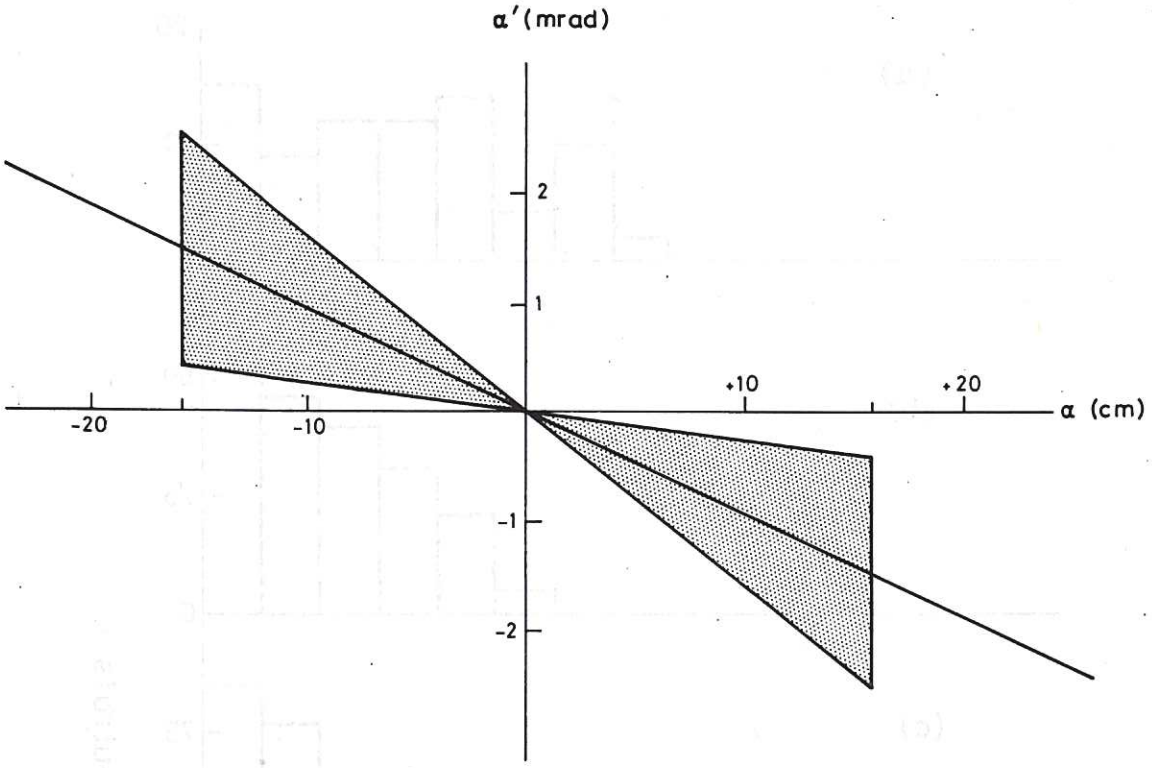

Fig.7 Phase-space (r, r') diagram of the JET neutral beam with $f_L = \infty$. The contour is at the 1/e-point on the particle distribution.

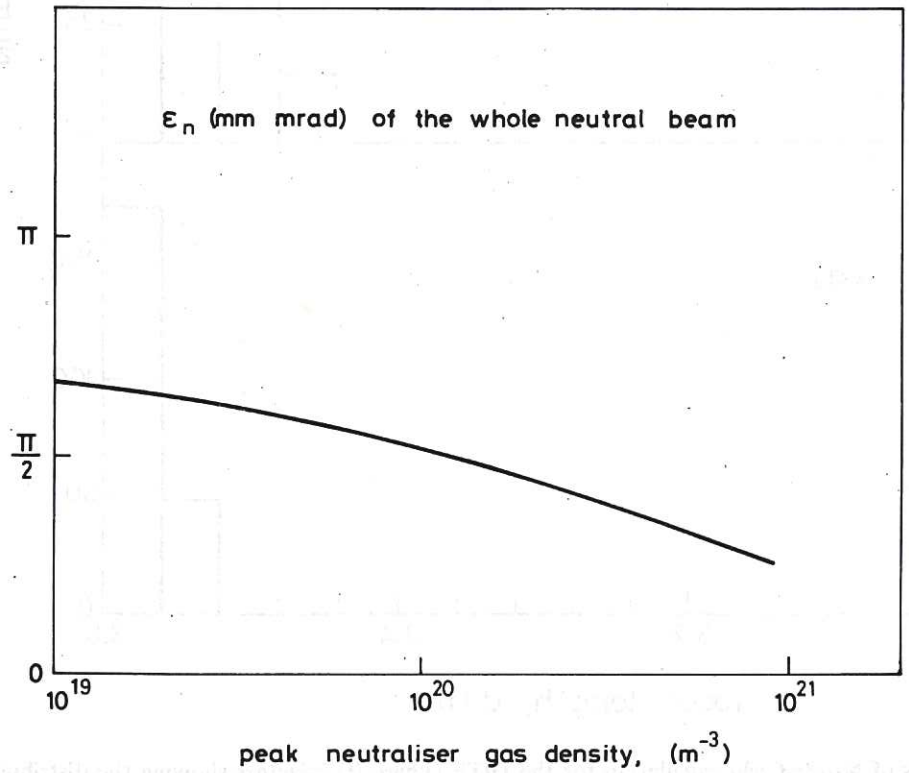

Fig.8 The phase-space area (enclosed by the 1/e-points on the neutral particle distribution function) in normalised emittance units plotted against peak gas density in the JET neutraliser.

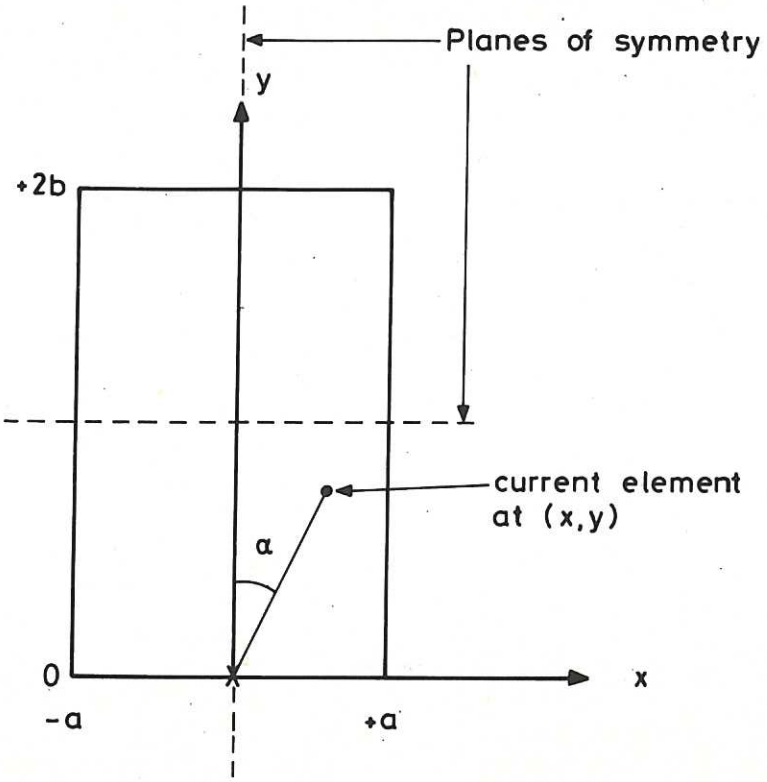

Fig.9 Geometry of the rectangular ion source in the plane of the extraction gap.

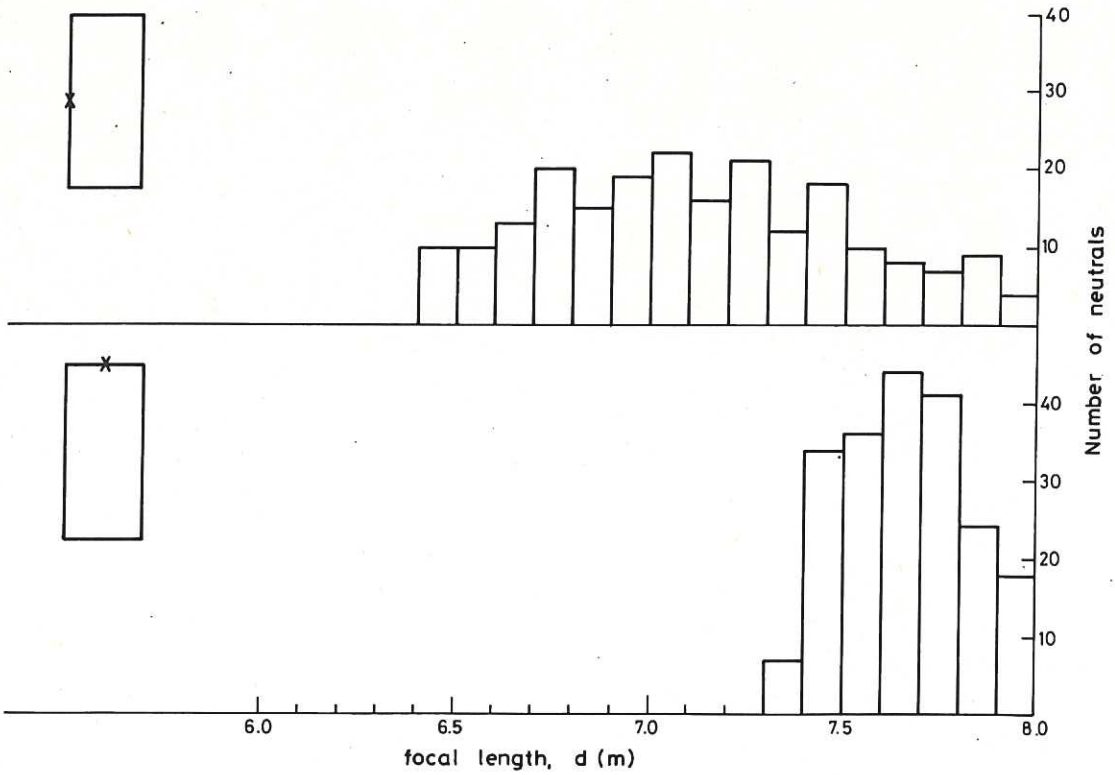

Fig.10 Results of Monte-Carlo calculation (JET case) for two test beamlet positions (shown in insets) giving the distribution of neutral particle foci in the two planes. The peak gas density in the neutraliser was $6{\cdot}4 \times 10^{19}$ m^{-3}.